Rehybridized 1,3-Butadiene Radical Cations: How Far Will a Radical Cation Go To Maintain Conjugation?

Jonas Oxgaard and Olaf Wiest*

Department of Chemistry and Biochemistry, University of Notre Dame, Notre Dame, Indiana 46556-5670

Received: January 9, 2002

As chemical investigations move into new fields, such as radical ions, the understanding of even fundamental reactions sometimes undergoes revisions. Here, the mechanisms for the interconversion of the *s-cis* and *s-trans* rotamers of several 1,3-butadiene radical cations are investigated with hybrid density functional theory and are shown to exhibit a complexity far exceeding rotamer interconversion in the neutral analogues. In particular, rehybridization of the central carbons during the interconversion process results in a two-parameter mechanism, where one parameter is the rotation around the central bond, and the other parameter is the rehybridization. To convert rotamers, the rehybridized centers must invert. The origin of this effect is traced to one of the most basic concepts in chemistry, conjugation. Substituent effects on the rehybridization and the rotation mechanism are studied by investigations of (2,3-X,X) disubstituted butadienes, where X = $-CH_3$, $-NH_2$, $-OH$, $-F$, $-SiH_3$. Cation-stabilizing substituents are found to reduce the rehybridization, ranging from negligible reduction for $-F$ to practically eliminated rehybridization for $-SiH_3$. The same behavior is also encountered in the simplest conjugated cation and radical, that is, allyl cation and allyl radical. The effect of rehybridization on classical transition state versus dynamic control of the reaction is discussed, as well as the suitability of using model studies when treating high-energy open-shell species.

Introduction

Conjugation is among the most important concepts in chemistry. Phenomena such as aromaticity, fluorescence, organic conductivity, and sigmatropic rearrangement are all directly caused by the delocalization of electrons.[1] Accordingly, the wealth of studies intended to characterize, explain, or apply the effects of conjugation accurately reflects the interest this concept holds for chemists.

One of the results of conjugation is the stabilization of spin or charge. Delocalizing spin or charge over several atoms not only yields resonance energy but also reduces Coulomb repulsion. The two most common examples of this are the allyl cation and allyl radical, which are textbook examples used to illustrate the concept of resonance theory.[1,2] A less-studied system, which nevertheless warrants attention, is the butadiene radical cation. Since these systems represent the smallest conceivable conjugated ionic/radical molecules, they are often used as model compounds for larger systems, ranging from systems with biological importance such as retinal[3] and the carotene radical cation[4] to industrially interesting systems such as conducting polymers.[5] Furthermore, conformations of these molecules found on the nonstationary parts of the potential-energy surface (PES) are often identified as moieties in intermediates of organic reactions. For example, it has been suggested that the ring opening of cyclobutene radical cation to butadiene radical cation goes through an intermediate closely resembling the transition state for 1,3-butadiene radical cation rotation.[6] Such nonstationary points are also important for the emerging view that reactions involving shallow wells, low barriers, or high-energy species, such as radical ions, are not governed by classic transition-state theory. Instead, dynamic factors control the outcome of the reactions, making a thorough understanding of the nonstationary parts of the PES a necessity.[7]

In linear olefins, the most commonly used method to assign qualitative resonance stabilization values is the examination of rotational barriers. Under the premise that no delocalization is present at the highest point of the rotational profile, the stabilization energy should be equal to the rotational barrier since the stabilizing orbital interaction vanishes for orthogonal orbitals. For radical ions there is an additional reason, as spin and charge must be localized in the transition structure to allow the olefin orbitals to change signs. Failure to do so would force continued rotation to occur on the excited-state surface.[6] Values obtained by this method are not quantitatively accurate, however, since other factors such as steric effects and σ-frame conjugation influence the barrier height.[8] There is also a possibility that the experimentally derived "rotational barrier" does not necessarily correspond to a rotation but could instead measure the activation energy of a series of isomerizations resulting in a product identical to the product of rotation. Wiberg et al. explored such a mechanism to explain the discrepancy between the experimentally derived rotational barrier of allyl cation, measured to be 20 kcal/mol, and the theoretical one calculated to be 30 kcal/mol.[9] Nevertheless, the rotational barrier height has been employed as a measure of conjugation in systems such as the allyl cation,[8−12] allyl radical,[8,11,13] allyl anion,[11,12,14] butadiene,[15,16] butadiene radical cation,[6,17] and derivatives thereof.[18,19]

The barrier height is but one part of the rotational profile, that is, the pathway leading from one rotamer to another. In the case of the neutral parent[15] and substituted[18,19] butadiene, entire rotational profiles have been investigated at various levels of theory. The knowledge ascertained in these studies has been used not only to understand conjugation but also for parametrization in force-field development and evaluation of quantum mechanical methods.[20] To the best of our knowledge, rotational

* To whom correspondence should be addressed. E-mail: owiest@nd.edu.

10.1021/jp020041c CCC: $22.00
Published on Web 03/26/2002

profiles have not been investigated for any of the other systems mentioned above.

During our work on hydrocarbon radical cations,[17,21] we encountered a behavior of the butadiene radical cation PES that did not agree with the common view of the geometric and electronic structure of radicals and cations. A cationic or radical carbon is, in the absence of steric constraints, assumed to be sp^2 hybridized.[1] In our investigation of the 1,3-butadiene radical cation, $\mathbf{1}^{\bullet+}$, this only appeared to be true at the stationary parts of the PES, that is, for the energy minima *syn*- and *anti*-$\mathbf{1}^{\bullet+}$ and the transition state connecting the two. Other points along the pathway connecting *syn*- and *anti*-$\mathbf{1}^{\bullet+}$, such as $\mathbf{1}^{\bullet+}$ with the carbon skeleton constrained to 50°, contain pyramidalized carbons and spin/charge residing on non-sp^2 hybridized carbons. More importantly, in the substituted butadiene radical cations where the minimum energy conformations were not planar, even stationary points on the PES displayed non-sp^2 hybridized carbons.

In this study, mechanisms for rotation of several 1,3-butadiene radical cations $\mathbf{1}^{\bullet+}-\mathbf{8}^{\bullet+}$ are investigated by theoretical methods. Furthermore, the smaller systems allyl cation and allyl radical are investigated to establish the relationship of these smaller and well-studied systems to the chemically more relevant butadienes. The following questions will be addressed: (i) What is the shape of the butadiene radical cation PES? (ii) How does a traditional, one-dimensional rotational profile describe a rehybridized molecule? (iii) What are the substituent effects on rehybridization and the mechanism of rotation? (iv) How do these results pertain to conjugated cations and radicals? (v) What effect does the rehybridization have for mechanistic consideration? (vi) Are these results transferable to larger systems such as the carotene radical cation?

Computational Methodology

All calculations were performed using the Gaussian 98 program package,[22] running on SGI Origin2000 and Origin3000 machines at the High Performance Computing Complex at the University of Notre Dame. Abbreviations used throughout this paper follow the ones used in Gaussian 98. Hybrid DFT calculations utilized Becke's three-parameter[23] (B3) functional combined with the correlation functional of Lee, Yang, and Par (LYP).[24] The double-ζ 6-31G* basis set developed by Pople and co-workers was used throughout the investigation except where noted.

As DFT is known to harbor inadequacies when describing symmetric radical cations,[6,25] for butadiene radical cations, these problems are confined to the transition structure.[17] Nevertheless, control calculations of $\mathbf{1}^{\bullet+}$ using the more reliable but computationally very demanding quadratic configuration interaction (QCI) method[26] with single and double excitations (QCISD) using the 6-31G* basis set, followed by single point QCISD(T) calculations with a 6-311G** basis set, abbreviated QCISD(T)/6-311G**//QCISD/6-31G*, were undertaken.

Notation in this publication follows the numbering scheme presented in Figure 1. The two significant dihedrals C1−C2−C3−C4 and X7−C2−C3−X8, where X7 and X8 are the substituents on C2 and C3, are labeled $\varphi 1$ and $\varphi 2$, respectively. A structure named $\mathbf{1}^{\bullet+}$ ($\varphi 1 = 90°$, $\varphi 2 = 37.2°$) would thus be molecule $\mathbf{1}^{\bullet+}$ with the dihedral angle C1−C2−C3−C4 equal to 90° and the dihedral angle H7−C2−C3−H8 equal to 37.2°.

Results

Unsubstituted Butadiene Radical Cation $\mathbf{1}^{\bullet+}$. The most stable conformation of $\mathbf{1}^{\bullet+}$ corresponds to the anti conformer

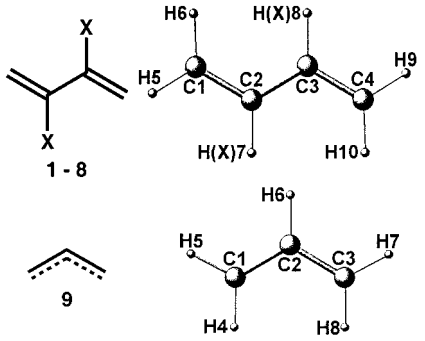

Figure 1. Compounds included in this study and their naming schemes. **1**: X = H, **2**: X = CH_3, **3**: X = NH_2, **4**: X = OH, **5**: X = F, **6**: X = SiH_3, **7**: X = CMe_3, **8**: X = $SiMe_3$.

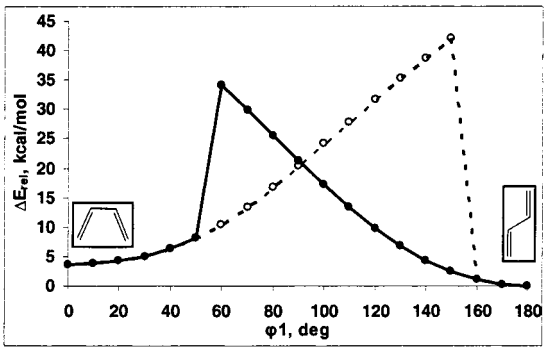

Figure 2. $\varphi 1$ scans of $\mathbf{1}^{\bullet+}$, starting from $\varphi 1 = 0°$ to $\varphi 1 = 180°$ (white points) and $\varphi 1 = 180°$ to $\varphi 1 = 0°$ (black points).

where the C1−C2−C3−C4 dihedral, labeled $\varphi 1$, is 180°. A second minimum corresponds to the syn conformer with $\varphi 1 = 0°$, 3.7 kcal/mol higher in energy at the B3LYP level of theory. Torsion potentials were initially investigated by fully optimizing the geometry of $\mathbf{1}^{\bullet+}$ with $\varphi 1$ constrained to fixed values, starting from 0° or 180°. For each new value of $\varphi 1$, the starting geometry was taken from the previous optimization. For example, the optimization of $\mathbf{1}^{\bullet+}$ ($\varphi 1 = 20°$) starts with a geometry taken from the optimized $\mathbf{1}^{\bullet+}$ ($\varphi 1 = 10°$). As will be discussed below, the initial geometry provides a bias for the optimization and therefore an optimization of $\mathbf{1}^{\bullet+}$ ($\varphi 1 = 90°$) starting from $\mathbf{1}^{\bullet+}$ ($\varphi 1 = 100°$) does not necessarily give the same geometry as an optimization started from $\mathbf{1}^{\bullet+}$ ($\varphi 1 = 80°$). Consequently, a potential where $\varphi 1$ was increased from 0° to 180° can be distinguished from a potential where $\varphi 1$ was decreased from 180° to 0°, labeled $\varphi 1_{0\rightarrow 180}$ and $\varphi 1_{180\rightarrow 0}$, respectively.

It is seen in Figure 2 that $\varphi 1_{0\rightarrow 180}$ is not equal to $\varphi 1_{180\rightarrow 0}$. After the crossing point at $\varphi 1 = 90°$, $\varphi 1_{0\rightarrow 180}$ continues on a higher energy surface until $\varphi 1_{0\rightarrow 180} = 150°$, after which it relaxes to the lower energy surface. $\varphi 1_{180\rightarrow 0}$ does likewise, continuing on a higher energy surface until $\varphi 1_{180\rightarrow 0} = 60°$.[27] The energies after relaxation differ less than 10^{-4} kcal/mol. The energy at the crossing point is 21.0 kcal/mol, significantly lower than the energy of the transition state for the rotation, ts-$\mathbf{1}^{\bullet+}$. Although this ts-$\mathbf{1}^{\bullet+}$ cannot be located by the B3LYP method, it has previously been located at the QCISD(T)/QCISD level, 28.1 kcal/mol higher in energy than the minimum energy conformer.[6,17] This discrepancy is far too large to be caused by overestimation of delocalization of DFT. Indeed, as will be discussed below, DFT yields energies that correspond very well to QCISD(T)/6-311G**//QCISD/6-31G* energies, and the reason for the 7.1 kcal/mol difference must thus be located elsewhere.

TABLE 1

	B3LYP/6-31G*					QCISD(T)/6-311G** / /QCISD/6-31G*		B3LYP/STO-3G		B3LYP/3-21G		B3LYP/6-31+G**	
a		C1−C2−	C4−C3−										
$\varphi 1$	$\varphi 2$	H7−C3	H8−C2	sp^x	ΔE	$\varphi 2$	ΔE	$\varphi 2$	ΔE	$\varphi 2$	ΔE	$\varphi 2$	ΔE
0°	0.0°	180.0°	180.0°	2.00	3.7	0.0°	3.6	0.0°	3.0	0.0°	3.5	0.0°	3.8
50° [a]	19.9°	165.8°	165.8°	2.24	8.1	19.2°	7.6	17.1°	8.8	20.4°	8.0	20.1°	8.1
70° [a]	27.8°	160.3°	160.3°	2.33	13.4	26.7°	13.0	25.3°	14.9	28.5°	13.3	28.2°	13.3
90° [a]	37.2°	156.4°	156.4°	2.39	21.4	35.4°	21.0	35.5°	22.4	38.1°	20.4	37.7°	20.2
90° [a]	70° [a]	170.6°	169.8°	2.17	24.3	70° [a]	26.7	70° [a]	26.7	70°[a]	24.2	70° [a]	24.0
90° [a]	90° [a]	180.0°	180.0°	2.00	28.7	90° [a]	28.1	90° [a]	32.2	90° [a]	29.5	90° [a]	29.3
90° [a]	110° [a]	170.2°	170.2°	2.16	24.2	110° [a]	23.2	110° [a]	27.0	110° [a]	24.1	110° [a]	23.9
90° [a]	140.7°	155.6°	155.7°	2.41	20.4	143.2°	20.4	142.8°	23.7	139.0°	21.5	140.1°	21.2
110° [a]	155.0°	158.1°	158.1°	2.37	13.3	156.2°	12.8	156.5°	14.9	153.3°	13.5	154.5°	13.2
130° [a]	165.0°	162.9°	162.9°	2.29	6.8	165.3°	6.4	166.0°	7.7	163.6°	7.0	164.5°	6.8
180°	180.0°	180.0°	180.0°	2.00	0.0	180.0°	0.0	180.0°	0.0	180.0°	0.0	180.0v	0.0

[a] Constrained dihedral. Relative energies in kcal/mol.

Upon closer analysis of the geometries obtained in the scan, the optimized geometries demonstrate pyramidalization of the central carbons C2 and C3. While the planar minima have the expected sp^2 hybridization, C2 and C3 attain partial sp^3 hybridization when $\varphi 1$ is distorted. It is also observed that the terminal carbon−carbon bonds are twisted, so that the dihedrals H5−C1−C2−H7 and H10−C4−C3−H8 are maintained at ∼180° throughout the scan, regardless of pyramidalization. The sp^3 hybridization is progressively more pronounced when $\varphi 1$ is increased. Rehybridization of C2 is intermediate between a pure sp^2 center, where the C1−C2−C3−H7 dihedral is 180°, and a pure sp^3 center, where the C1−C2−C3−H7 dihedral is 120°.[28] Thus, at $\varphi 1$=110°, where the C1−C2−C3−H7 dihedral is 158.1°, C2 could be considered an $sp^{2.37}$ center.[29] However, for visualization purposes it is beneficial to consider the H7−C2−C3−H8 dihedral, labeled $\varphi 2$, instead of the pyramidalization. In purely sp^2 hybridized carbons, $\varphi 2$ is equal to $\varphi 1$. When pyramidalization occurs, this is no longer true, as $\varphi 2$ is geometrically related to the distortion of planarity.[30] The C1−C2−C3−H7 dihedrals, sp^x hybridization and $\varphi 2$ dihedrals, are shown in Table 1.

As DFT has a well-known tendency to overestimate conjugation,[25] we investigated the possibility that the rehybridization could be a computational artifact of the methods used. Several points on the $\mathbf{1}^{\bullet+}$ PES were optimized at the QCISD(T)/6-311G**//QCISD/6-31G* level of theory. As can be seen in the results presented in Table 1, it is clear that these high level MO and the B3LYP calculations correspond very well to each other. Deviations from planarity differ less than 3°, although with a slight but persistent overestimation by B3LYP, consistent with the tendency of B3LYP to overestimate conjugation. The relative energies are within 1 kcal/mol of the QCISD(T) single-point energies, clearly indicating that B3LYP performs adequately in treating this system. Although DFT methods are known to be relatively basis-set independent,[17] it was also decided to explore different basis sets at the B3LYP level. Deviation from planarity is largely unaffected, deviating at most 4° between the basis sets. Relative energies are also unaffected, with the exception of the minimal basis set STO-3G, which overestimated the energy of the distorted geometries. The simple basis set 3-21G reproduced both geometries and energies accurately, however, suggesting that even fairly large molecules could be treated adequately with this smaller basis set.

In Table 1, two structures with $\varphi 1 = 90°$ are listed, corresponding to $\varphi 1_{0\rightarrow 180} = 90°$ and $\varphi 1_{180\rightarrow 0} = 90°$. With $\varphi 2$ values of 37.2° and 140.7°, respectively, there is an obvious discrepancy. Intuitively, to convert $\varphi 1_{0\rightarrow 180} = 90°$ to $\varphi 1_{180\rightarrow 0} = 90°$, $\mathbf{1}^{\bullet+}$ must pass through a geometry where $\varphi 2 \approx$ 90°, illustrated in Figure 3. Indeed, the QCISD ts-$\mathbf{1}^{\bullet+}$ geometry has $\varphi 1 = 89.9°$ and $\varphi 2 = 86.7°$. A scan from $\varphi 2 = 0°$ to $\varphi 2 = 180°$, with $\varphi 1$ frozen to 90°, was undertaken. The rotational profile obtained from this scan, presented in Figure 4, show a peak at $\varphi 1 = 90°$ and $\varphi 2 = 90°$, 28.7 kcal/mol higher in energy than *anti*-$\mathbf{1}^{\bullet+}$. The relative energy as well as geometry of this peak conforms well to the QCISD(T)/UHF ts-$\mathbf{1}^{\bullet+}$ at 29.4 kcal/mol. The full mechanism of this process is thus first a rotation of $\varphi 1$ from 0° to 90°, during which $\varphi 2$ goes from 0° to 37.2°. In other words, as the central carbon−carbon bond rotates toward $\varphi 1 = 90°$, pyramidalization of C2 and C3 increases continuously, to maintain conjugation. After $\varphi 1$ has reached 90°, $\varphi 2$ is rotated toward 90° as well. At $\varphi 1 \approx 90°$, $\varphi 2 \approx 90°$, the molecule localizes spin and charge on one of the two olefinic moieties to flip the orbital sign on the other olefin and continues downhill on the other part of the PES. The minimum energy path undergoes a rotation of $\varphi 2$ until it reaches 140.7°, at which point the rotation of $\varphi 1$ from 90° to 180° occurs.

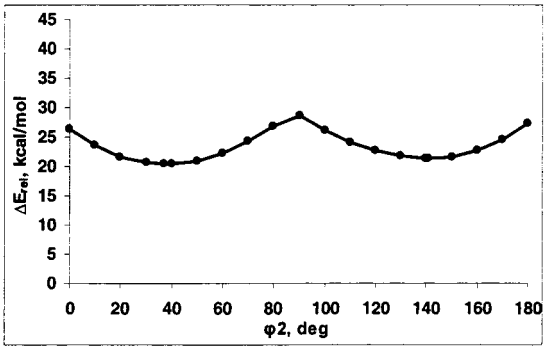

Figure 3. $\varphi 2$ scan of $\mathbf{1}^{\bullet+}$ with $\varphi 1$ frozen at 90°.

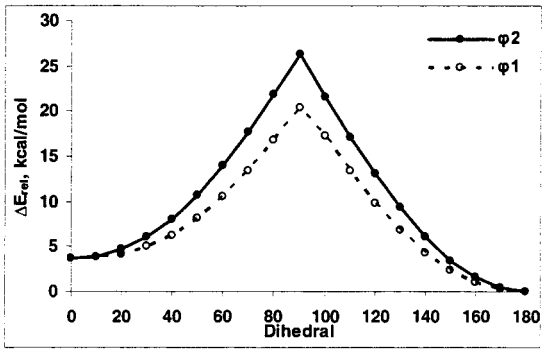

Figure 4. $\varphi 2$ scan of $\mathbf{1}^{\bullet+}$ overlaid with $\varphi 1$ scan.

The energy minima of the scan in Figure 3 are encountered at $\varphi 2 = 37.2°$ and $\varphi 2 = 140.7°$. The lack of further minima

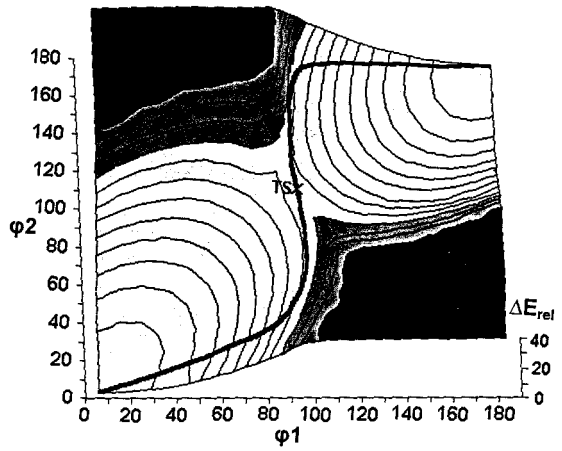

Figure 5. PES of $\mathbf{1}^{\bullet+}$. Each contour line corresponds to 3 kcal/mol. Minimum energy pathway is shown in bold.

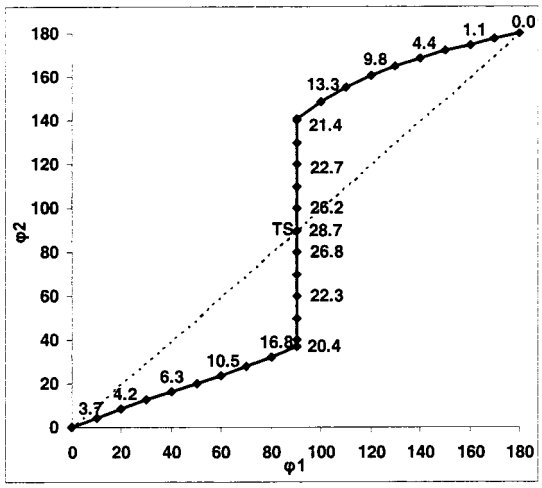

Figure 6. Reduced PES of $\mathbf{1}^{\bullet+}$. Relative energies are in kcal/mol.

indicates that the complimentary mechanism, where $\varphi 2$ would first be rotated from 0° to 90°, followed by rotation of $\varphi 1$ past 90°, and then $\varphi 2$ again from 90° to 180°, is not energetically competitive. To validate this, a scan of $\varphi 2$ from 0° to 180° was undertaken and the results from this calculation are shown in Figure 4, overlaid with the earlier $\varphi 1$ scan. It is clear that rotating $\varphi 1$ is energetically more favorable by ~6 kcal/mol.

To ensure that no other alternative pathways are present, a more complete mapping of the PES was undertaken, where $\mathbf{1}^{\bullet+}$ structures with $\varphi 1 = 0°, 10°, ..., 170°, 180°$; $\varphi 2 = 0°, 10°, ..., 170°, 180°$ were optimized. The results are shown in Figure 5, where also the energies presented in Figures 2 and 4 are overlaid in a bold line, representing the lowest energy pathway from *syn*- to *anti*-$\mathbf{1}^{\bullet+}$. Relative energies above 40 kcal/mol are left out to enhance visibility of the more pertinent parts of the PES, while parts of the PES higher than 30 kcal/mol are shaded dark gray. The mechanism can thus be described as a steady twisting of $\varphi 1$ until it reaches 90°, at which point $\varphi 2$ is twisted. At $\varphi 1 = 90°$, $\varphi 2 = 90°$, a localization of spin and charge occurs and the butadiene relaxes onto the other side of the PES. The bold line indeed represents the lowest energy path on the PES, and thus no competing minimum energy pathway appears to be present.

In the absence of competing paths on the PES, the representation of the mechanism can be reduced to Figure 6, where $\varphi 1$ is plotted versus $\varphi 2$. Since this requires less than 30 data points, as opposed to the 18^2 required to fit the PES, this represents a drastic reduction in the required computational effort. Thus, all further mechanisms, bar one, will be discussed using $\varphi 1$ versus $\varphi 2$ plots.

Substituent Effects. As the rehybridization occurs to increase stabilization of spin and charge, the obvious question is how does this pertain to larger, more chemically relevant systems? As almost all larger systems stabilize the spin and charge by substituents, a systematic substituent effect survey was undertaken. 2,3-(X,X) disubstituted butadiene radical cations, where X = $-CH_3$, $-NH_2$, $-OH$, $-F$, $-SiH_3$ labeled $\mathbf{2}^{\bullet+}$ to $\mathbf{6}^{\bullet+}$, respectively, were investigated using the methodology described above.[32] The chosen substituents stabilize spin and charge in the order $-H < -F < -CH_3 < -OH < -NH_2 < -SiH_3$, as judged by their σ^+ and $\sigma^\bullet$ values. $\varphi 1$ versus $\varphi 2$ plots of $\mathbf{2}^{\bullet+}$ to $\mathbf{5}^{\bullet+}$ are presented in Figure 7. $\mathbf{2}^{\bullet+}$ follows the same mechanism as $\mathbf{1}^{\bullet+}$, although with a lower activation energy, 18.5 kcal/mol at the QCISD(T)/6-31G*//UHF/6-31G* level. Similar to the case of $\mathbf{1}^{\bullet+}$, the transition structure could not be located at the B3LYP level of theory. The degree of pyramidalization is lower than observed for $\mathbf{1}^{\bullet+}$, with an average deviation from planarity of 20.1°, compared to 27.0° for $\mathbf{1}^{\bullet+}$. The irregularity observed between $\varphi 1 = 130°$ and $\varphi 1 = 140°$ is due to reduction of steric interaction between the methyl groups and the allyl hydrogens.

The syn and anti isomerization of $\mathbf{3}^{\bullet+}$ follows a slightly different pathway. The minimum energy conformers can be found at ($\varphi 1 = 25.0°$, $\varphi 2 = 15.1°$) and ($\varphi 1 = 126.8°$, $\varphi 2 = 135.7°$), the latter being 1.4 kcal/mol higher in energy. Consequently, there will be three transition states on the PES, two of which will invert the pyramidalization of C2 and C3. The third transition state, responsible for interconversion of the minima, could not be located with any method. However, a CASSCF(3,4) conical intersection optimization puts a conical intersection at ($\varphi 1 = 69.6°$, $\varphi 2 = 69.3°$). The highest point on the B3LYP PES is found at ($\varphi 1 = 71.7°$, $\varphi 2 = 60.0°$) and thus seems to correspond fairly well to the expected location of the transition state. The barrier to interconversion, which is estimated to be ≈10 kcal/mol, is substantially lower than the corresponding barrier for $\mathbf{1}^{\bullet+}$. The pyramidalization is also much less pronounced, deviating on average only 13.2° from planarity.

The minimum energy conformers for $\mathbf{4}^{\bullet+}$ can be found at ($\varphi 1 = 153.8°$, $\varphi 2 = 158.9°$) and ($\varphi 1 = 0°$, $\varphi 2 = 0°$). The latter minimum is stabilized by a hydrogen bond and is thus 6.9 kcal/mol more stable than the anti minimum. As the hydrogen bond is not present in the transition state, all energies are relative to the anti minimum. The transition structure is found at $\varphi 1 = 74.5°$, $\varphi 2 = 74.5°$, 12.8 kcal/mol higher in energy than the anti minimum. Clearly, the orbitals in the transition structure are not orthogonal. This is most likely due to steric reasons, which are becoming more important as the conjugative stabilization of spin and charge decrease. The pyramidalization is less pronounced than for $\mathbf{1}^{\bullet+}$ but more so than in the case of $\mathbf{3}^{\bullet+}$, with an average deviation from planarity of 18.5°. Furthermore, the degree of pyramidalization actually decreases from $\varphi 1 = 90°$ to $\varphi 1 = 74.5°$, indicating that the energy gained by increased conjugation is not enough to offset the energy lost through pyramidalization.

The PES computed for $\mathbf{5}^{\bullet+}$, also shown in Figure 7, is very similar to the $\mathbf{1}^{\bullet+}$ PES. The 25.7 kcal/mol barrier to interconversion at the QCISD(T)/UHF level is slightly lower than the barrier for $\mathbf{1}^{\bullet+}$, as expected for the slightly higher cation-stabilizing character of fluorine over hydrogen.[33] The degree of pyramidalization is also slightly lower, with an average deviation from planarity of 25.5°. For compounds $\mathbf{2}^{\bullet+}$ to $\mathbf{5}^{\bullet+}$, alternative pathways, that is, twisting of $\varphi 2$ and non-rehybridized

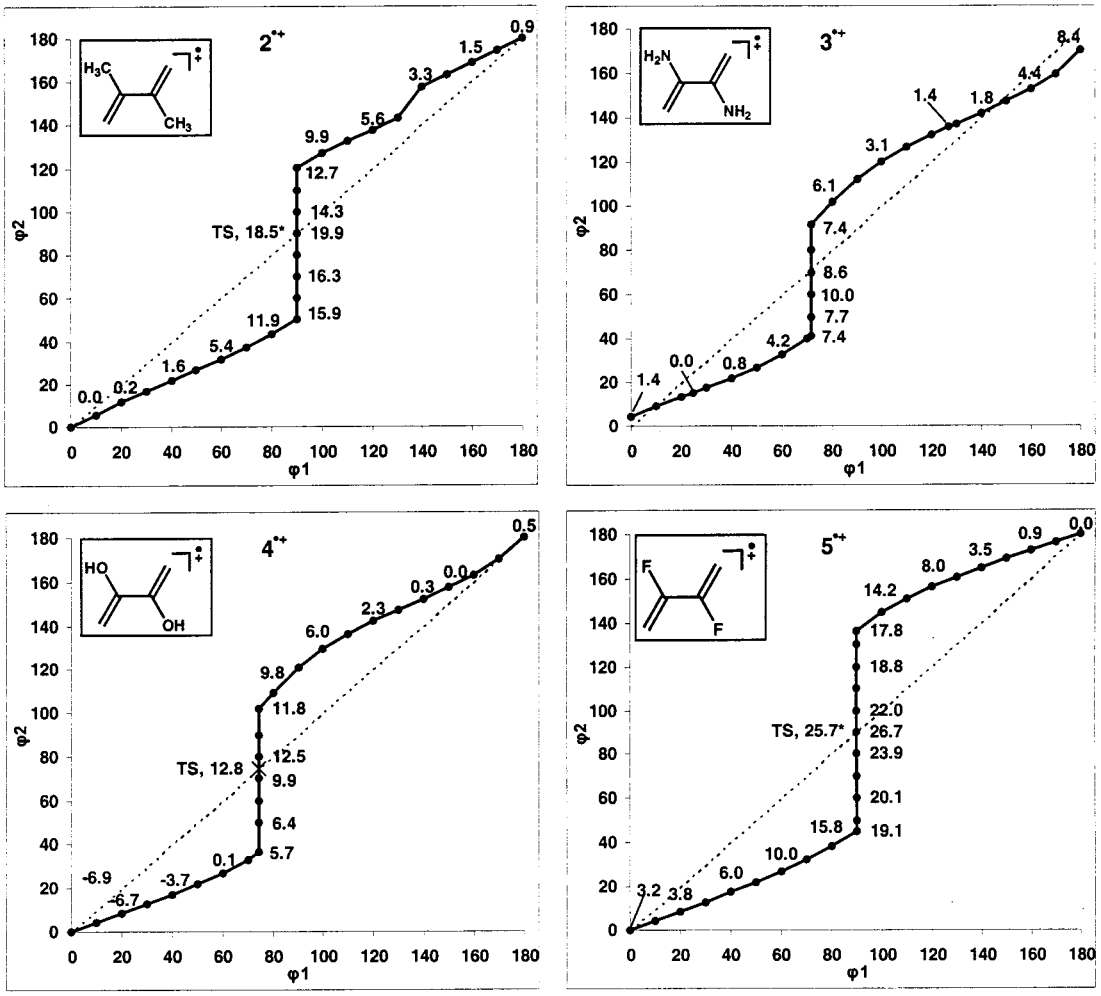

Figure 7. Reduced PES of $\mathbf{2}^{\bullet+}$−$\mathbf{5}^{\bullet+}$. Relative energies are in kcal/mol.

$\varphi1/\varphi2$ scans, were evaluated and found to be higher in energy than the $\varphi1$ pathway and were thus not pursued further.

The minimum energy conformers of $\mathbf{6}^{\bullet+}$ are located at ($\varphi1 = 180°$, $\varphi2 = 180°$) and ($\varphi1 = 29.2°$, $\varphi2 = 22.3°$). The interconversion transition structure, ts-$\mathbf{6}^{\bullet+}$, is located at ($\varphi1 = 93.7°$, $\varphi2 = 89.6°$), 8.8 kcal/mol above *anti*-$\mathbf{6}^{\bullet+}$. A $\varphi1$ scan reveals a low degree of pyramidalization, with an average deviation of 11° from planarity. The control scan of $\varphi2$, however, gave an alternative path that is energetically competitive with $\varphi1$. From the gauche minimum to ts-$\mathbf{6}^{\bullet+}$, the $\varphi1$ path is the minimum pathway, although at most 1.3 kcal lower than the $\varphi2$ path, $\varphi1$ is also the minimum from ts-$\mathbf{6}^{\bullet+}$ to $\varphi = 110°$, at which point $\varphi2$ becomes the lower minimum pathway. However, the difference between the paths is at most 0.2 kcal/mol and is thus below the accuracy of the method used. With an ambiguous mechanism such as this, it felt necessary to map the entire PES, which is presented in Figure 9. Relative energies above 13 kcal/mol have been left out to enhance visibility, and energies above 9 kcal/mol are shaded dark gray. The resulting PES is somewhat different from the smoothly curved PES presented for $\mathbf{1}^{\bullet+}$ in Figure 5. The region around the diagonal is very flat, while the curvature increases steeply when leaving the flat area, indicating that the energy gained through increased delocalization does not offset the energy lost through pyramidalization.

The final pair of butadienes studied, the *tert*-butyl substituted $\mathbf{7}^{\bullet+}$ and the trimethylsilyl substituted $\mathbf{8}^{\bullet+}$, were chosen not only for the electronic properties of the substituents but also for their steric effects, which lead to an unusual structure that differs considerably from normal 1,3-butadienes. The double bonds in the neutral analogue **7** are essentially orthogonal because of the steric bulk of the *tert*-butyl groups.[19] Assuming that $\mathbf{7}^{\bullet+}$ has a similar geometry, it can be used as a probe of whether minimum energy conformers of butadiene radical cations also exhibit rehybridization. In $\mathbf{7}^{\bullet+}$, the minimum energy conformer is located at ($\varphi1 = 123.2°$, $\varphi2 = 134.1°$), with a second minimum at ($\varphi1 = 53.2°$, $\varphi2 = 60.1°$), 3.0 kcal/mol higher in energy. The twist of $\varphi1$ from 89.9° in **7** to 123.2° in $\mathbf{7}^{\bullet+}$ is due to the tendency to delocalize spin and charge in the radical cation. The computed structure of $\mathbf{7}^{\bullet+}$ is thus an interesting example

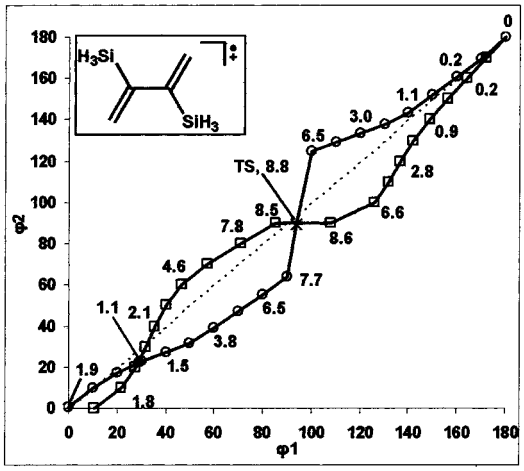

Figure 8. Reduced PES of $\mathbf{6}^{\bullet+}$. Relative energies are in kcal/mol.

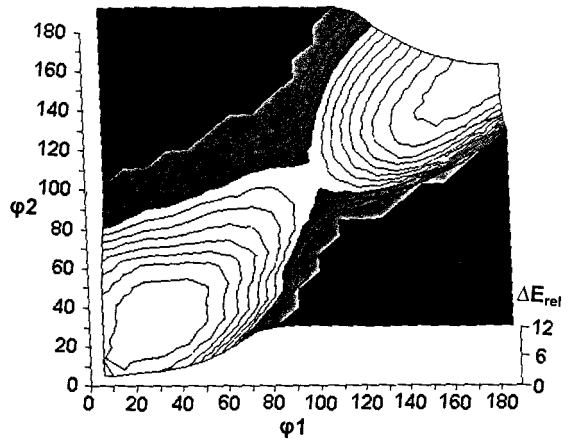

Figure 9. PES of $\mathbf{6}^{\bullet+}$. Each contour line corresponds to 3 kcal/mol.

of the delicate balance between the steric repulsion of the *tert*-butyl groups and the stabilization of spin and charge in a radical cation.

While the pyramidalization in the ($\varphi1 = 53.2°$, $\varphi2 = 60.1°$) minimum should be caused by strain, the pyramidalization in the ($\varphi1 = 123.2°$, $\varphi2 = 134.1°$) causes the *tert*-butyl groups to come closer, that is, increasing strain. However, in **7** with $\varphi1$ constrained to 53.2°, $\varphi2$ is equal to 78.1°, thus exhibiting substantially more pyramidalization than $\mathbf{7}^{\bullet+}$ ($\varphi1 = 53.2°$, $\varphi2 = 60.1°$). Conversely, the substituents in $\mathbf{8}^{\bullet+}$ have similar steric bulk as the ones in $\mathbf{7}^{\bullet+}$, yet $\mathbf{8}^{\bullet+}$ exhibits negligible pyramidalization in the minimum energy conformer at ($\varphi1 = 136.2°$, $\varphi2 = 135.3°$). This is not surprising, in the light of the reduction of pyramidalization when comparing $\mathbf{2}^{\bullet+}$ to $\mathbf{6}^{\bullet+}$.

Allyl Cation and Allyl Radical. As radical cations have been successfully treated as the combination of a radical and a cation,[34] the question arose whether conjugated radicals or cations would exhibit similar rehybridization. The rotation of the methylene group in the allyl cation, $\mathbf{9}^{+}$, and allyl radical, $\mathbf{9}^{\bullet}$, were chosen as the simplest model of conjugated cations and radicals. As discussed earlier, these model systems had considerable impact on the development of the fundamental concept of conjugation. Comparison of the situation in $\mathbf{9}^{+}$ and $\mathbf{9}^{\bullet}$ with the ideas outlined above therefore puts them in the context of established concepts. To investigate this, the methylene group on C3 was rotated by constraining the C1−C2−C3−H7 dihedral to 180°, then decreasing it to 90° in 10° increments. The energy profile and pertinent dihedrals are given in Figure 10.

Similar to the butadiene radical cations, rotation of the methylene moiety in $\mathbf{9}^{+}$ causes pyramidalization of C3. With C1−C2−C3−H7 set to 90°, the C2−C3−H8−H7 dihedral, that is, the out-of-plane bending of C3, is 151.6° and 22.9 kcal/mol higher in energy than planar $\mathbf{9}^{+}$. Furthermore, C2 is also pyramidalized to a slightly larger extent with the C1−C2−C3−H6 dihedral equal to 139.9°. Analogous calculations of the allyl radical $\mathbf{9}^{\bullet}$ revealed a different pattern for pyramidalization. With C1−C2−C3−H7 set to 90°, 17.0 kcal/mol higher in energy than planar $\mathbf{9}^{\bullet}$, the C2−C3−H8−H7 dihedral is 154.4°, but the C1−C2−C3−H6 dihedral is only 173.5°. The differences in rehybridization of C2 can be traced to differences in localization of spin or charge. Mulliken partial charges in planar $\mathbf{9}^{+}$ are calculated to 0.39, 0.21, and 0.39 electrons at C1, C2, and C3, respectively, and changes to 0.33, 0.25, and 0.42 electrons, respectively, in $\mathbf{9}^{+}$ with C1−C2−C3−H7 = 90°. Therefore, the electronic structure of $\mathbf{9}^{+}$ is largely unchanged during the

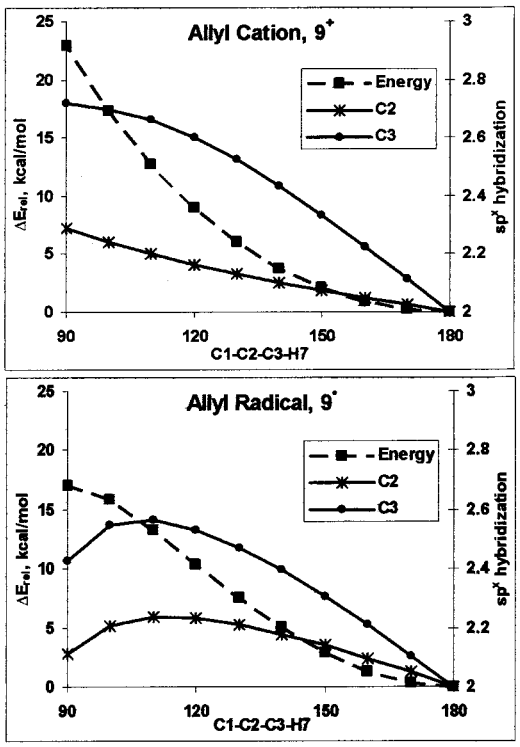

Figure 10. a: Energy and sp^x hybridization at C2 and C3 in scan of $\mathbf{9}^{+}$. b: Energy and sp^x hybridization at C2 and C3 in scan of $\mathbf{9}^{\bullet}$.

rotation. In $\mathbf{9}^{\bullet}$, on the other hand, the spin density on C1, C2, and C3 goes from 0.63, (−0.26), and 0.63, respectively, in planar $\mathbf{9}^{\bullet}$ to 0.09, (−0.07), and 0.98, respectively, in $\mathbf{9}^{\bullet}$ with C1−C2−C3−H7 = 90°. Furthermore, in $\mathbf{9}^{\bullet}$ with C1−C2−C3−H7 = 108°, the spin density is 0.33, (−0.21), and 0.87, respectively, indicating that there is still substantial delocalization in $\mathbf{9}^{\bullet}$ (C1−C2−C3−H7 = 108°) but no delocalization present in $\mathbf{9}^{\bullet}$ (C1−C2−C3−H7 = 90°). The decreasing degree of pyramidalization calculated for $\mathbf{9}^{\bullet}$ between (C1−C2−C3−H7 = 108°) and (C1−C2−C3−H7 = 90°) is caused by the energetic cost of rehybridizing C2 which exceeds the gain from maintained conjugation in this range. This in turn should cause $\mathbf{9}^{\bullet}$ to behave in a classical fashion, which is also supported by the agreement between the experimental and calculated barriers to rotation.

Discussion and Conclusions

Conversion of *syn*- to *anti*-$\mathbf{1}^{\bullet+}$ is a much more complicated process than previously thought and differs considerably from the rotation in neutral **1**. The main reason for this is the rehybridization of the central carbons C2 and C3 that occurs when the geometry is distorted from planarity, which leads to larger stabilization of spin and charge. The driving force for this is the increased overlap between the two formerly pure p-orbitals afforded by rehybridization. If the partially pyramidalized carbons have perfect tetrahedral geometry, at $\mathbf{1}^{\bullet+}$ ($\varphi1 = 90°$, $\varphi2 = 37.2°$) the dihedral angle between the former p-orbitals on C2 and C3 should be (90° + 37.2°)/2 = 63.6°. A dihedral angle of 63.6° is significantly less than 90° and is thus exhibiting overlap.[35] The energy difference between $\mathbf{1}^{\bullet+}$ ($\varphi1 = 90°$, $\varphi2 = 37.2°$) and $\mathbf{1}^{\bullet+}$ ($\varphi1 = 90°$, $\varphi2 = 90°$) of 8.3 kcal/mol is the stabilization due to delocalization minus the energy required to pyramidalize the carbons. As introducing cation-stabilizing substituents at the central carbons simultaneously reduces both the degree of rehybridization and the barrier to

interconversion, it is clear that the degree of rehybridization is dependent on the energy gained by it. While delocalization is dependent on electronic factors, the rehybridization is not.

The effect of rehybridization on the butadiene radical cation PES is evident from Figures 5 to 9. The rotamer interconversion is dependent on not only a geometric parameter, that is, the torsion of $\varphi 1$, but also an electronic parameter, that is, the rehybridization. As the second parameter is perpendicular to the reaction coordinate $\varphi 1$, the interconversion is expected not to follow classical transition-state theory but instead to be dynamically controlled. In the most extreme example, interconversion of unsubstituted butadiene would by following the minimum energy pathway reach the ($\varphi 1 = 90°$, $\varphi 2 = 37.2°$) geometry. To pass through the transition structure, it would have to stop the $\varphi 1$ twisting motion and instead start a new, independent motion. This is unlikely, and a large portion of the ($\varphi 1 = 90°$, $\varphi 2 = 37.2°$) geometries would instead continue twisting $\varphi 1$ until they eventually rehybridized. A geometry passing through a point ($\varphi 1 = 110°$, $\varphi 2 = 90°$) would still have to localize spin and charge, however, and would thus have what might be called a nonstationary transition state. The minimum energy pathways presented in Figures 5−9 are consequently not describing the exact mechanism but instead give a most likely pathway for interconversion. The minimum energy pathway does provide information about the PES, however, as a pathway such as the one presented in Figure 6, where the rehybridization is substantial, is expected to exhibit a large degree of nonclassical behavior. A minimum energy pathway such as the one presented in Figure 8, on the other hand, is indicative of a PES where the pathways leading to interconversion are fairly close to a one-parameter surface, following the diagonal. This system is thus expected to be well described within the classical transition-state theory.

The rehybridization is not limited to radical cations, however, as seen by the rotation of allyl cation and to a lesser extent allyl radical. Just as observed for the substituent effects, the lesser degree of rehybridization for allyl radical is consistent with a lower energy gain through delocalization and thus a lower driving force to maintain it. Although not explored, the rehybridization in $\mathbf{9}^+$ could explain the absence of a C_{2h} symmetric rotational transition state,[9] as this transition state could ostensibly be found in the three-dimensional space shaped by the rotation of the C2−C3 bond and the pyramidalization of C2 and C3. It is also possible, however, that the previously suggested 1,2-hydrogen shift[9] might occur at a twisted geometry, lower in energy than the C_{2h} symmetric 1,2-hydrogen shift characterized by Wiberg et al.[9] Furthermore, it is expected to influence the energetics and geometry of other mechanisms, such as allyl radical to allene eliminations.

Rehybridization is also important in energy minima on the PES, provided that those conformers are nonplanar and do not contain strongly cation-stabilizing substituents. This is exemplified by $\mathbf{7}^{\bullet+}$, where the *tert*-butyl groups in $\mathbf{7}^{\bullet+}$ are bulky but not strongly cation-stabilizing. The system has a minimum energy conformer where the double bonds are not planar, but pyramidalization of the central carbons is present. $\mathbf{8}^{\bullet+}$ is nonplanar, but the trimethylsilyl substituents are highly cation-stabilizing, and $\mathbf{8}^{\bullet+}$ has thus no driving force for pyramidalization.

The performance of the B3LYP model is in very good agreement to computationally much more demanding methods. This is particularly relevant for the parent system, the rotation of butadiene radical cation $\mathbf{1}^{\bullet+}$. The failure of the B3LYP method to locate the transition structure for the rotation of $\mathbf{1}^{\bullet+}$ has often been interpreted as an indication that this method is unreliable. Our results demonstrate that a much more differentiated view of the shortcomings of these hybrid DFT methods, which describe the vast majority of the hypersurfaces very well, is necessary. Although the origins of the bias in the B3LYP method is well understood, a full understanding of the consequences will require further studies of several systems.

The results described here are of considerable generality. This is, for example, emphasized by a more detailed consideration of a butadiene-like radical cation that is strongly stabilized by substituents, the carotene radical cation. On the basis of the discussion above, the rotation of carotene radical cation is expected to exhibit small deviations from the classical behavior. Rotation of the headgroups of the carotene radical cation was the object of a recent theoretical study.[36] A closer analysis of the structure that was twisted by 90° reveals a small degree of rehybridization on the relevant carbons. The effect this has on the rotational profile is most likely negligible but nevertheless clearly present. More importantly, however, this demonstrates the dangers of using model studies. While in this case a flawed model of a larger species can be discarded on the basis of an examination for nonclassical behavior, this is not always the case.

Acknowledgment. We gratefully acknowledge financial support of this research by the Volkswagen Foundation (I/72 647) and the National Science Foundation (CHE97-33050) and allocation of computational resources by the OIT at the University of Notre Dame. J. Oxgaard thanks the Department of Chemistry and Biochemistry for funding provided through the Reilly fellowship. We also wish to thank Dr. Thomas Bally for his assistance in explaining the pitfalls of computational organic radical cation chemistry.

Supporting Information Available: Tables of absolute energies, pertinent dihedrals, and QCISD(T) absolute energies are available free of charge via the Internet at http://pubs.acs.org. Geometries and other data can be obtained from the authors upon request.

References and Notes

(1) See, for example, Jones, M. *Organic Chemistry*; W. W. Norton & Company: New York, 1997.

(2) Wheland, G. W. *Resonance in Organic Chemistry*; Wiley: New York, 1955.

(3) See, for example, Garavelli, M.; Bernardi, F.; Robb, M. A.; Olivucci, M. *J. Mol. Struct. (THEOCHEM)* **1999**, *464*, 59.

(4) See, for example: Keszthelyi, T.; Wilbrandt, R.; Bally, T. *J. Mol. Struct.* **1997**, *410*, 339.

(5) (a) Bally, T.; Roth, K.; Tang, W.; Schrock, R. R.; Knoll, K.; Park, L. Y. *J. Am. Chem. Soc.* **1992**, *114*, 2440. (b) Bushby, R. J.; McGill, D. R.; Ng, K. M.; Taylor, N. *Chem. Commun.* **1996**, 2641. (c) Shirakawa, H. *Angew. Chem., Int. Ed.* **2001**, *40*, 2574. (d) MacDiarmid, A. G. *Angew. Chem., Intl. Ed.* **2001**, *40*, 2581. (e) Heeger, A. J. *Angew. Chem., Intl. Ed.* **2001**, *40*, 2591.

(6) Sastry, G. N.; Bally, T.; Hrouda, V.; Carsky, P. *J. Am. Chem. Soc.* **1998**, *120*, 9323.

(7) Carpenter, B. K. *Angew. Chem., Intl. Ed.* **1998**, *37*, 3340. (b) Bolton, K.; Hase, W. L.; Doubleday, C. *J. Phys. Chem. B* **1999**, *103*, 3691 (c) Doubleday, C.; Nendel, M.; Houk, K. N.; Thweatt, D.; Page, M. *J. Am. Chem. Soc.* **1999**, *121*, 4720. (d) Nicoll, R. M.; Hillier, A. H.; Truhlar, D. G. *J. Am. Chem. Soc.* **2001**, *123*, 1459. (e) Doubleday, C. *J. Phys. Chem. A* **2001**, *105*, 6333.

(8) Mo, Y.; Lin, Z.; Wu, W.; Zhang, Q. *J. Phys. Chem.* **1996**, *100*, 6469.

(9) Foresman, J. B.; Wong, M. W.; Wiberg, K. B.; Frisch, M. J. *J. Am. Chem. Soc.* **1993**, *115*, 2220.

(10) (a) Mayr, H.; Forner, W.; Schleyer, P. v. R. *J. Am. Chem. Soc.* **1979**, *101*, 6032. (b) Rahavachari, K.; Whiteside, R. A.; Pople, J. A.; Schleyer, P. v. R. *J. Am. Chem. Soc.* **1981**, *103*, 5649. (c) Cournoyer, M. E.; Jorgensen, W. L. *J. Am. Chem. Soc.* **1984**, *106*, 5104.

(11) (a) Gobbi, A.; Frenking, G. *J. Am. Chem. Soc.* **1994**, *116*, 9275. (b) Mo, Y.; Lin, Z.; Wu, W.; Zhang, Q. *J. Phys. Chem.* **1996**, *100*, 6469.

(12) (a) Wiberg, K. B.; Breneman, C. M.; LePage, T. J. *J. Am. Chem. Soc.* **1990**, *112*, 61. (b) Mo, Y.; Peyerimhoff, S. D. *J. Chem. Phys*. **1998**, *109*, 1687.

(13) (a) Feller, D.; Davidson, E. R.; Borden, W. T. *J. Am. Chem. Soc.* **1984**, *106*, 2513. (b) Karadakov, P. B.; Gerratt, J.; Raos, G.; Cooper, D. L.; Raimondi, M. *J. Am. Chem. Soc.* **1994**, *116*, 2075.

(14) Clark, T.; Rohde, C.; Schleyer, P. v. R. *Organometallics* **1983**, *2*, 1344.

(15) Wiberg, K. B.; Rosenberg, W. K. B.; Rablen, P. R. *J. Am. Chem. Soc.* **1991**, *113*, 2890. (b) Karpfen, A.; Choi, C. H.; Kertesz, M. *J. Phys. Chem. A* **1997**, *101*, 7426.

(16) (a) Pratt, L. R.; Hsu, C. S.; Chandler, D. *J. Chem. Phys*. **1978**, *68*, 4202. (b) Squillacote, M. E.; Sheridan, R. S.; Chapman, O. L.; Anet, F. A. L. *J. Am. Chem. Soc*. **1979**, *101*, 3657. (c) Herrebout, W. A.; van der Veken, B. J.; Wang, A.; Durig, J. R. *J. Phys*. *Chem*. **1995**, *99*, 578. (d) Murcko, M. A.; Castejon, H.; Wiberg, K. B. *J. Phys. Chem*. **1996**, *100*, 16162.

(17) Oxgaard, J.; Wiest, O. *J. Phys. Chem. A* **2001**, *105*, 8236.

(18) (a) Tsuzuki, S.; Schaefer, L.; Hitoshi, G.; Jemmis, E. D.; Hosoya, H.; Siam, K.; Tanabe, K.; Osawa, E. *J. Am*. *Chem*. *Soc*. **1991**, *113*, 4665. (b) Karpfen, A. *J. Phys. Chem. A* **1999**, *103*, 2821.

(19) (a) Traetteberg, M.; Hopf, H.; Lipka, H.; Hanel, R. *Chem. Ber*. **1994**, *127*, 1459. (b) Traetteberg, M.; Bakken, P.; Hopf, H.; Hanel, R. *Chem. Ber*. **1994**, *127*, 1469.

(20) (a) Maxwell, D. S.; Tirado-Rives, J.; Jorgensen, W. L. *J. Comput. Chem*. **1995**, *16*, 984. (b) Halgren, T. A. *J. Comput. Chem*. **1996**, *17*, 490. (c) Allinger, N. L.; Chen, K.; Li, J.-H. *J. Comput. Chem*. **1996**, *17*, 642.

(21) (a) Wiest, O. *J. Am. Chem. Soc*. **1997**, *119*, 5713. (b) Saettel, N.; Oxgaard, J.; Wiest, O. *Eur. J. Org. Chem.* **2001**, *8*, 1429.

(22) Frisch, M. J.; Trucks, G. W.; Schlegel, H. B.; Scuseria, G. E.; Robb, M. A.; Cheeseman, J. R.; Zakrzewski, V. G.; Montgomery, J. A., Jr.; Stratmann, R. E.; Burant, J. C.; Dapprich, S.; Millam, J. M.; Daniels, A. D.; Kudin, K. N.; Strain, M. C.; Farkas, O.; Tomasi, J.; Barone, V.; Cossi, M.; Cammi, R.; Mennucci, B.; Pomelli, C.; Adamo, C.; Clifford, S.; Ochterski, J.; Petersson, G. A.; Ayala, P. Y.; Cui, Q.; Morokuma, K.; Malick, D. K.; Rabuck, A. D.; Raghavachari, K.; Foresman, J. B.; Cioslowski, J.; Ortiz, J. V.; Stefanov, B. B.; Liu, G.; Liashenko, A.; Piskorz, P.; Komaromi, I.; Gomperts, R.; Martin, R. L.; Fox, D. J.; Keith, T.; Al-Laham, M. A.; Peng, C. Y.; Nanayakkara, A.; Gonzalez, C.; Challacombe, M.; Gill, P. M. W.; Johnson, B. G.; Chen, W.; Wong, M. W.; Andres, J. L.; Head-Gordon, M.; Replogle, E. S.; Pople, J. A. *Gaussian 98*, revision A.9; Gaussian, Inc.: Pittsburgh, PA, 1998.

(23) Becke, A. D. *J. Chem. Phys.* **1993**, *98*, 5648.

(24) Lee, C.; Yang, W.; Parr, R. G. *Phys. Rev. B* **1988**, *37*, 785.

(25) (a) Barnett, R. N.; Landman, U. *J. Phys. Chem.* **1995**, *99*, 17305. (b) Hrusak, J.; Friedrichs, H.; Schwarz, H.; Razafinjanahary, H.; Chermette, H. *J. Phys. Chem.* **1996**, *100*, 100. (c) Hiberty, P. C. In *Modern Electronic Structure Theory and Applications in Organic Chemistry*; Davidson, E. R., Ed.; World Scientific: River Edge, NJ, 1997; p 289. (d) Hrouda, V.; Roeselová, M.; Bally, T. *J. Phys. Chem. A* **1997**, *101*, 3925. (e) Bally, T.; Sastry, G. N. *J. Phys. Chem. A* **1997**, *101*, 7923. (f) Braïda, B.; Hiberty, P. C. *J. Phys. Chem. A* **1998**, *102*, 7872. (g) Sodupe, M.; Bertran, J.; Rodriguez-Santiago, L.; Baerends, E. J. *J. Phys. Chem. A* **1999**, *103*, 166. (h) Chermette, H.; Ciofini, I.; Mariotti, F.; Daul, C. *J. Chem. Phys.* **2001**, *114*, 1447.

(26) Pople, J. A.; Head-Gordon, M.; Raghavachari, K. *J. Chem. Phys.* **1987**, *87*, 3700.

(27) The scan was also repeated with the Gaussian keyword guess = always, thus creating a new wave function for each step of the optimization. The result remained unchanged. As the computational time required increased by a factor of 10, this was only done for testing purposes.

(28) The dihedral angle C1−C2−C3−H7 is defined as the angle between the planes formed by C1−C2−C3 and C2−C3−H7 and will thus measure with what angle the C2−H7 bond bends out of the C1−C2−C3 plane. There are two other possible dihedral angles, C1−C2−H7−C3 and C1−H7−C2−C3, which are nonequal. The difference between the angles is at most 3°, and we will thus confine the discussion to the C1−C2−C3−H7 dihedral.

(29) Sp^x hybridization is here treated as the linear mixture of an sp^2 center with a C1−C2−H7−C3 dihedral of 180° and an sp^3 center with a C1−C2−H7−C3 dihedral of 120°. If the measured dihedral is Y, then $Y = 120°*(x - 2) + 180°(1 - (x - 2))$. Solving for x gives $x = 2 + (180° - Y)/60°$. A center with a dihedral of 160° would thus be an $sp^{2.33}$ center.

(30) Between $\varphi 1 = 0°$ and $\varphi 1 = 90°$, $\varphi 2 = \varphi 1 - (180° - \varphi_{(C1-C2-H7-C3)}) - (180° - \varphi_{(C4-C3-H8-C2)})$. Between $\varphi_1 = 90°$ and $\varphi_1 = 180°$, $\varphi_2 = \varphi_1 + (180° - \varphi_{(C1-C2-H7-C3)}) + (180° - \varphi_{(C4-C3-H8-C2)})$.

(31) The energies obtained by QCISD/6-31G* show differences as large as 10 kcal/mol when compared to the B3LYP or QCISD(T)/6-311G** single-point energies of the QCISD/6-31G* geometry. This discrepancy increased dramatically with more pronounced pyramidalization and will be the topic of a forthcoming publication.

(32) Compound **4** is not experimentally accessible, as it undergoes a facile tautomerization to the corresponding diacyl species. As the purpose of this study is to establish a substituent effect trend rather than an investigation of individual compounds, it was decided to use **4** instead of the stable 2,3-(MeO, MeO) 1,3-butadiene.

(33) Isaacs, N. *Physical Organic Chemistry*, 2nd ed.; Wiley: New York, 1995.

(34) (a) Wang, Y.; McLean, K. H.; Tanko, J. M. *J. Org. Chem.* **1998**, *63*, 628. (b) Herbertz, T.; Blume, F.; Roth, H. D. *J. Am. Chem. Soc.* **1998**, *120*, 4591. (c) Herbertz, T.; Roth, H. D. *J. Am. Chem. Soc.* **1998**, *120*, 11904. (d) Herbertz, T.; Roth, H. D. *J. Org. Chem.* **1999**, *64*, 3708. (e) Tanko, J. M.; Philips, J. P. *J. Am. Chem. Soc.* **1999**, *121*, 6078.

(35) This can best be illustrated by a Newman projection along the C2−C3 axis. The formerly pure p-orbital on C2 is 120° from both H7 and C1, and the formerly pure p-orbital on C3 is 120° from H8 and C4. Using $\mathbf{1}^{\bullet+}$ ($\varphi 1 = 90°$, $\varphi 2 = 37.2°$) as an example, the p-orbitals have a dihedral angle of 63.6°.

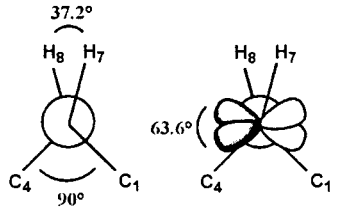

(36) Himo, F. *J. Phys. Chem. A* **2001**, *105*, 7933.